ACS Macro Letters

November 2018 • Volume 7, Issue 11

pubs.acs.org/acsmacrolett

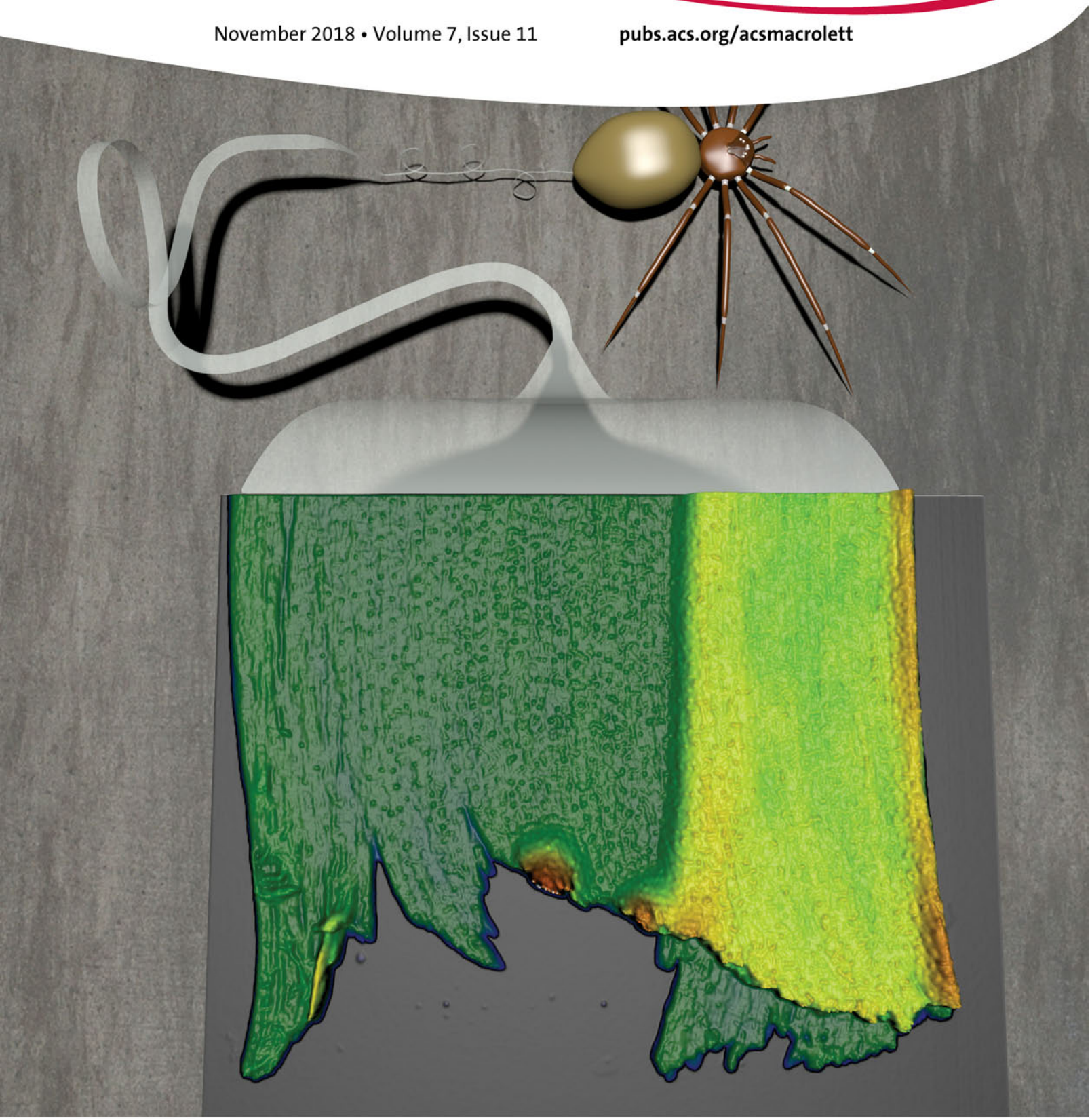

ACS Publications
Most Trusted. Most Cited. Most Read.

www.acs.org

ACS Macro Letters

Letter

Cite This: ACS Macro Lett. 2018, 7, 1364−1370

pubs.acs.org/macroletters

Strength of Recluse Spider's Silk Originates from Nanofibrils

Qijue Wang and Hannes C. Schniepp*

Applied Science Department, The College of William and Mary, P.O. Box 8795, Williamsburg, Virginia 23187-8795, United States

Supporting Information

ABSTRACT: Spider silk exhibits a combination of outstanding tensile strength and extensibility unique among all synthetic and biogenic polymer fibers. It has thus generated great interest to understand protein-based high-toughness materials and inspired the design of similar synthetic materials. The unrivaled properties of silk fibers have been recognized to be intimately related to their hierarchical structure. However, in the absence of unambiguous experimental evidence, competing and incompatible structural models of natural silk fibers have been proposed, some of them including various types of fibrillar components. Here we show that the fibers of the recluse (*Loxosceles*) spider exhibit the typical tensile properties of a very good spider silk and are entirely composed of 20 nm diameter protein fibrils that are more than 1 μm long. Based on these findings, we developed the most detailed structural model for any silk directly supported by experimental evidence. Our work suggests that all the key properties of a spider silk are implemented within a single nanofibril, and we have isolated and imaged such a nanofibril from a native spider silk fiber. The nanofibril breaking force was estimated to be ≈120 nN. Our work underlines the importance of nanofibrils and furthers the understanding of the structure−property relationships of silk, with wide-ranging implications for silk research and the design of silk-inspired high-performance materials.

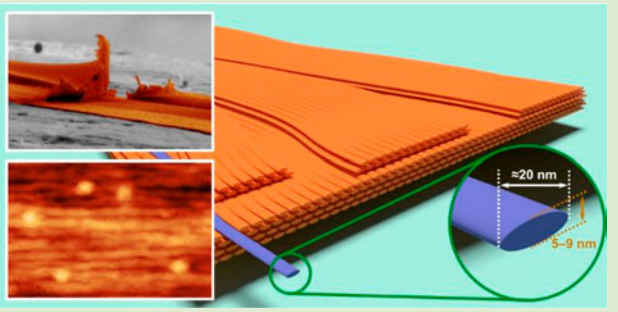

Spider silk is one of the strongest and toughest natural materials and has attracted great interest.[1,2] However, despite significant efforts, an experimentally confirmed consensus model of its hierarchical structure has remained elusive. For some of the dominating structural materials in the living world based on cellulose[3] or collagen,[4] it has been shown that nanofibrils are at the origin of their mechanical performance.[5−7] For spider silk, nanofibrils have been widely speculated to play an important role, however, so far without satisfying experimental support. The prevalence and exact dimensions of the hypothesized nanofibrils in native spider silks remain undetermined; no isolated nanofibrils have been detected. Here we present the first example of a natural spider silk fiber that is entirely composed of nanofibrils, yet displays all the mechanical properties of a strong and tough silk. The nanofibrils are uniform, featuring cross-sectional dimensions of ≈7 nm × 20 nm, which allowed us, for the first time, to estimate the mechanical properties of spider silk nanofibrils, with potentially wide-ranging implications for the understanding of the structure−property relationships of silk.

Previous attempts to detect spider silk nanofibrils have employed electron,[8,9] atomic force (AFM),[10−12] and optical[9,13,14] microscopy on cylindrical silk fibers. Nanofibrils have been observed on the surface of both spider[8,12,15] and silkworm silk,[16−18] with diameters of 20−80 nm. However, since the silk surface only accounts for a small volumetric fraction of the entire fiber, these results cannot provide information regarding nanofibrils in the bulk of silk fibers. To expose the interior of spider silk fibers and determine their structure, chemical or physical sample treatments have been used, leading to the observation of internal nanofibrils with diameters of 100−200 nm,[9,10,13,14,19] significantly larger than fibrils observed on the fiber surface. This discrepancy may be due to the harsh sample treatments employed, potentially altering the material.

Isolated nanofibrils of native spider silk have never been detected, let alone characterized. Notably, Ling et al.[20] chemically exfoliated silkworm fibers and found nanofibrils with ≈20 nm diameter; however, like in all reports on nanofibrils, no information on whether they represent a significant volume fraction of the fiber was provided. In absence of clear experimental evidence showing internal nanofibrils in silk fibers, some groups have suggested that silk is predominantly composed of micellar or granular building blocks.[11,21−23]

Here we have studied the major ampullate (MA) silk of the recluse spider (*Loxosceles* genus, Figure 1a), which the spider extrudes through a unique flattened nozzle (Figure 1b,c), thus, featuring a morphology different from all other known spider silks, a high aspect ratio ribbon, 45−65 nm thin and 6−8 μm wide (Figure 1d).[24−26] Due to its extreme thinness, virtually all of the fiber material is exposed on the surface, and thus, complete characterization of the material's structure using surface-based methods is possible. Figure 1e features higher-resolution AFM data acquired on native *Loxosceles* ribbons showing closely packed linear structures that are oriented strictly

Received: September 6, 2018
Accepted: October 22, 2018

DOI: 10.1021/acsmacrolett.8b00678
ACS Macro Lett. 2018, 7, 1364−1370

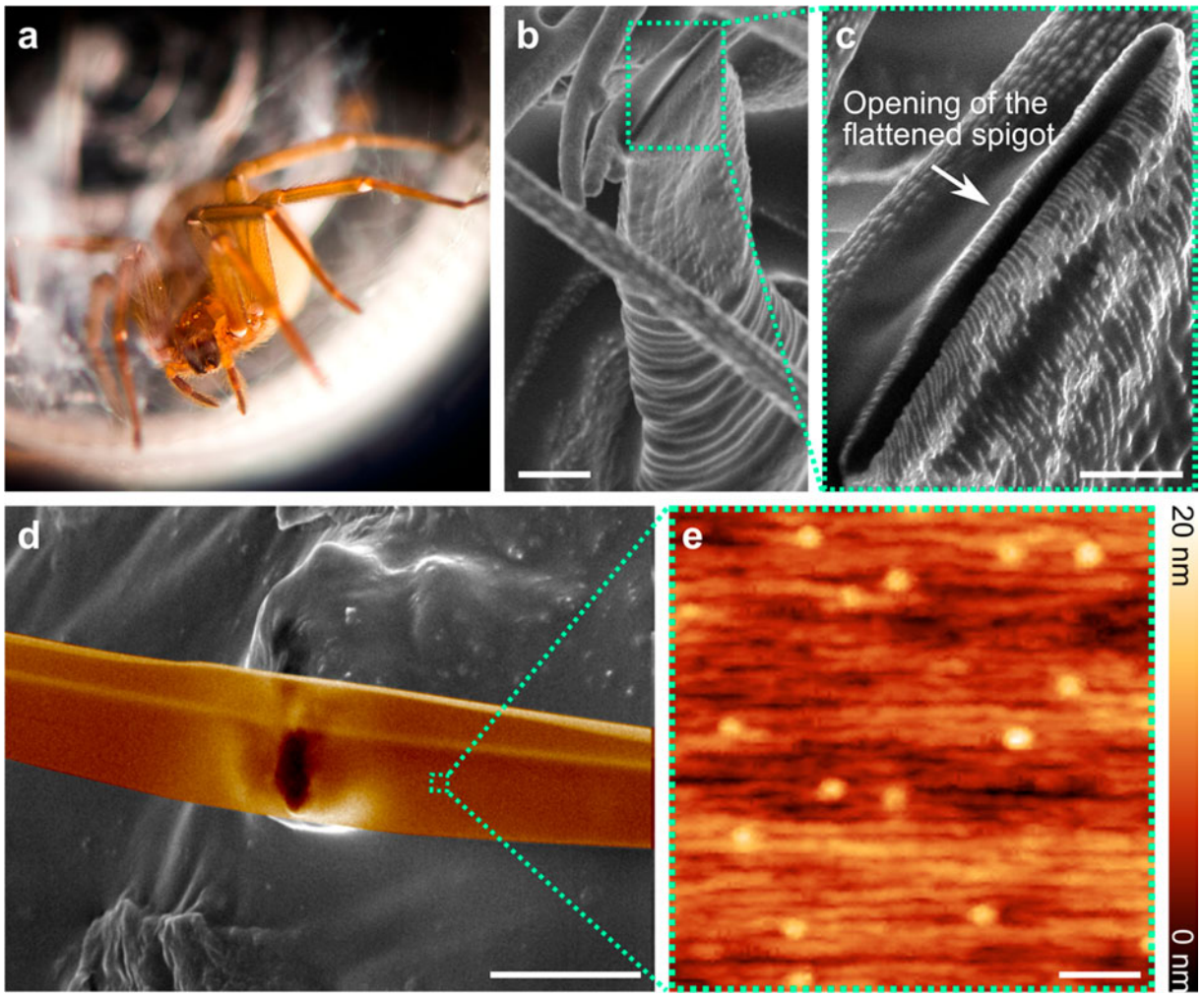

Figure 1. (a) *Loxosceles laeta* spider. (b, c) Flattened *Loxosceles* spigot from which silk ribbons are extruded (SEM). (d) False-colored SEM overview image of a *Loxosceles* ribbon placed on carbon tape. (e) Tapping-mode AFM topography of the ribbon surface. Scale bars: (b) 5 μm; (c) 2 μm; (d) 5 μm; (e) 100 nm.

parallel to the fiber direction and essentially account for all material on the surface. Figure 1e also exhibits dot-like surface protrusions previously termed "nanopapillae".[24] In contrast to our previous work, the AFM evidence shown here clearly revealed the presence of nanofibrils as individual, distinct elements (Figure 1e). Their width was determined as 21.3 ± 3.3 nm (n = 50) via AFM topography sections of close-packed nanofibrils (details in the Supporting Information). The measured widths are in excellent agreement with previously reported dimensions for surface nanofibrils on fibers from silkworm,[16,18] spider[15] and synthetic silks.[22] In terms of surface structure and texture, *Loxosceles* silk is thus indeed similar to all other silks. Our goal was to determine whether the thin *Loxosceles* ribbons are entirely made out of nanofibrils or if there is another structural component located between the surfaces.

Our tests to find an additional structural component below the surface of the ribbons employed several methods. First, we stretched a silk ribbon to failure and imaged the fracture surface via AFM (Figure 2a). The brighter region on the right side of Figure 2a represents a region where one part of the ribbon was tucked under during sample preparation, thus doubling the apparent thickness. The average thickness of this individual ribbon was 57.5 ± 4.5 nm (n = 10), measured via AFM topography sections across the ribbon edge (see details in Figure S3). Interestingly, in at least five areas in Figure 2a, indicated by yellow arrows, the topography at the fractured ribbon edge does not decrease abruptly, but in a stepped fashion (see details in the inset of Figures 2a and S4), hinting at a layered ribbon makeup. The presence of distinct layers was further supported by the structure of surface defects we observed in a small number of silk ribbons. Figure 2b features an AFM phase image of the lower part of an oval-shaped opening exposing nanofibrils in the layer underneath (inset: topography image showing the entire defect). The topmost layer of fibrils was seemingly torn open and moved laterally. Based on this defect and other evidence highlighted in Figure S5 (Supporting Information), we assessed the thickness of a single nanofibril layer to be 6.9 ± 2.3 nm. Consequently, this silk ribbon is ≈6−11× as thick as the surface layer.

To visualize the interior ribbon structure below the surfaces shown in Figures 1 and 2, an AFM probe was used to systematically remove a portion of silk on the ribbon surface, an approach recently used for AFM-based 3D tomography.[27] We scratched the silk ribbon with enough force to penetrate the surface, albeit with less force than would be required to penetrate the fiber all the way to the substrate (Figure 3). AFM topography and optical microscopy images of the resulting long, narrow trench, with an orientation perpendicular to the fiber axis

DOI: 10.1021/acsmacrolett.8b00678
ACS Macro Lett. 2018, 7, 1364−1370

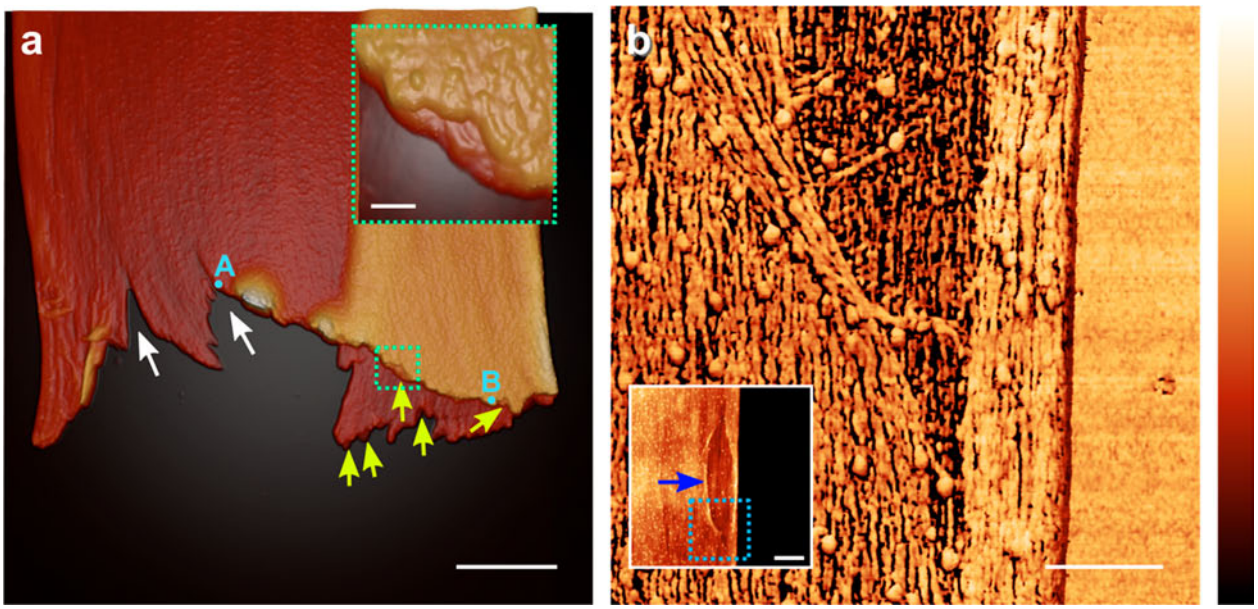

Figure 2. (a) 3D-rendered AFM topography of ruptured silk ribbon, folded underneath itself in the right part of the image. Inset: Ruptured ribbon featuring a stepped edge. Other locations showing such steps are indicated by yellow arrows. (b) AFM phase image showing part of a surface defect. Inset: Topography image of the examined surface defect (blue arrow). Light blue dotted box: location of panel (b). Scale bars: (a) 1 μm, inset: 100 nm; (b) 200 nm, inset: 500 nm. Color bar: (a) and its inset: 0−200 nm; (b) +15° to −55°, inset: 40−70 nm (0 nm representing the average height of the substrate).

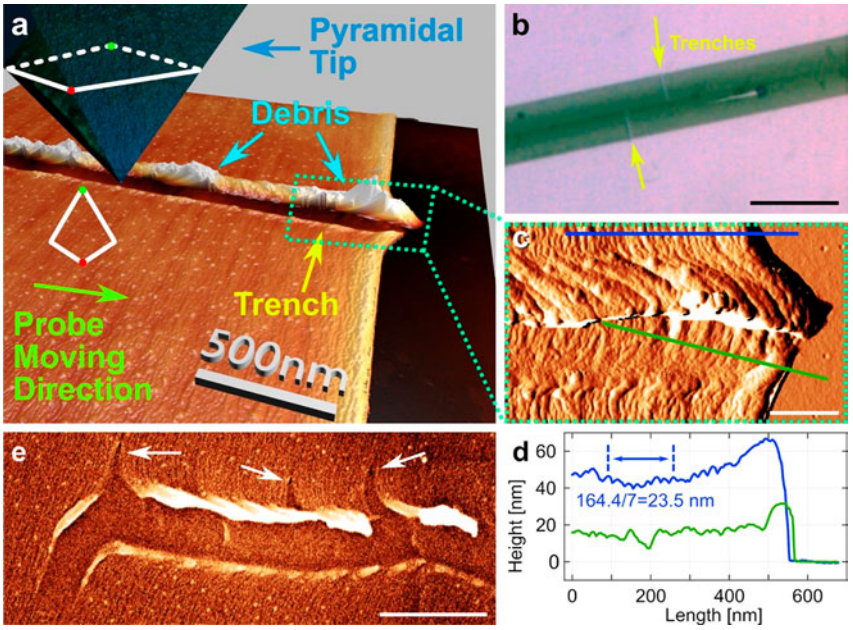

Figure 3. (a) 3D-rendered AFM topography with superimposed, schematic representation of AFM probe. Because of probe asymmetry (kite-shaped cross-section indicated as overlay), debris was mainly deposited on one side of the trench. (b) Optical microscope image of ribbon after scratching, with yellow arrows indicating the trenches. (c) Magnitude image of the area in the green dotted box in panel (a), showing nanofibrils inside the trench. These nanofibrils are oriented at an angle because of "AFM scratching". (d) Cross-sectional profiles taken from locations indicated in panel (c) in corresponding colors. (e) SEM image of one trench taken immediately after scratching. Ends of nanofibrils can be identified pointing away from the surface. Scale bars: (b) 10 μm; (c) 200 nm; (e) 1 μm.

are shown in Figure 3a,b. The close-up magnitude image shown in Figure 3c revealed parallel nanofibrils underneath the surface, with dimensions and orientation similar to the superficial nanofibrils. The nanofibrils in the trench were 17.6 ± 1.5 nm (n = 10) wide, slightly less than superficial fibrils (see Figure S6 for details), which could be due to sample distortions incurred upon scratching. As Figure 3a,c show, the debris produced via AFM scratching was predominantly located on one side of the trench, as expected from the shape of the AFM probes employed (see Figure 3a and more details in the Supporting Information).

To evaluate the depth of the scratched trench, two topography sections were prepared (see Figure 3d), one in the trench (green) and one on the pristine fiber (blue), with positions indicated in matching colors in Figure 3c. Apparently, the

DOI: 10.1021/acsmacrolett.8b00678
ACS Macro Lett. 2018, 7, 1364−1370

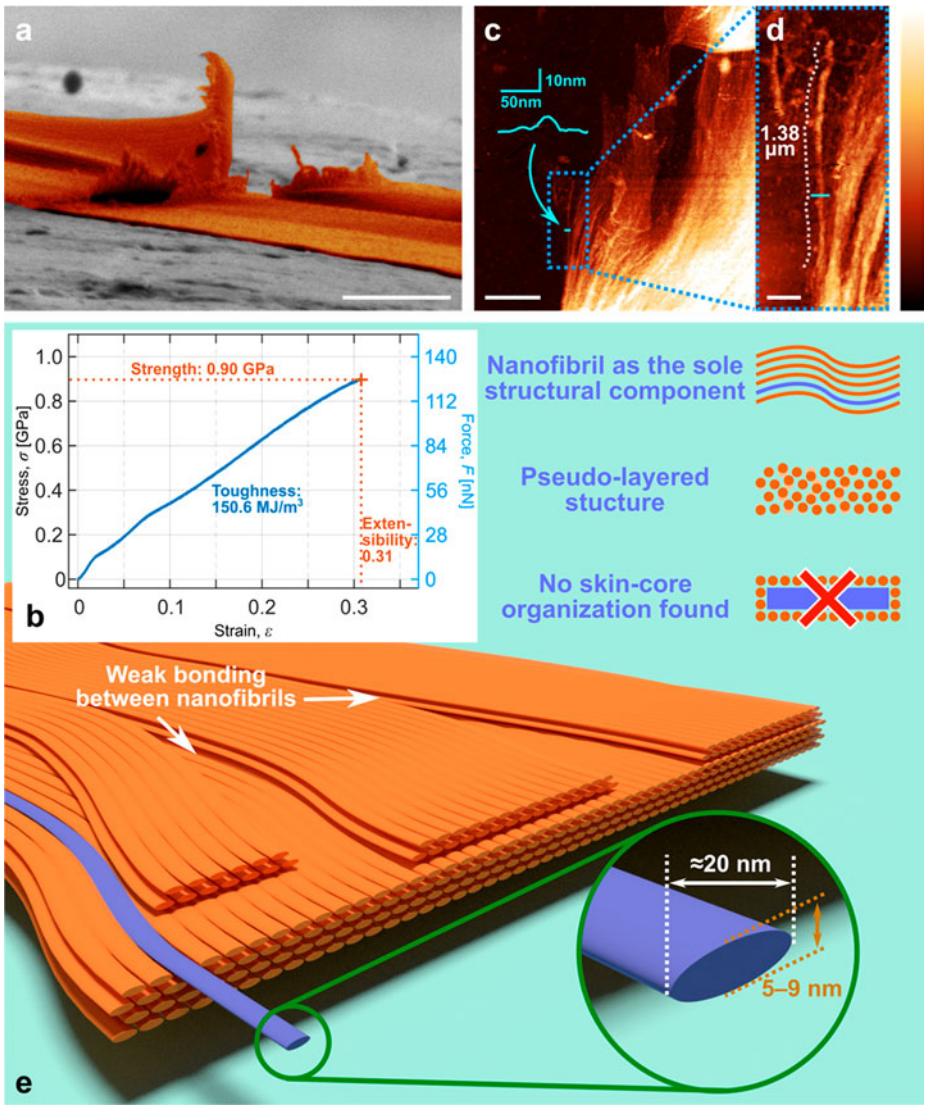

Figure 4. (a) In situ SEM image taken after cutting a ribbon (false-colored) using a focused ion beam (FIB) featuring numerous individual nanofibrils pointing away from the fracture site. (b) Stress−strain curve of a *Loxosceles* MA silk strand. The values of strength, extensibility, and toughness are comparable to a typical dragline silk. Right vertical axis: average force applied per individual nanofibril. (c, d) Exposed nanofibrils of a *Loxosceles* ribbon following partial dissolution (AFM topography). The fibril indicated by the white dashed line has a length of 1.38 μm. A topography cross-section and its location on the isolated nanofibril are shown with scales in cyan color. (e) Scheme of structural organization of a *Loxosceles* silk ribbon. This is the first time that this level of structural organization has been determined for any silk. Scale bars: (a) 1 μm; (c) 1 μm; (d) 200 nm. Color bar: (c) 0−60 nm, (d) 0−30 nm.

thickness of the material remaining in the trench after scratching is a little less than 20 nm on average, approximately half of the original thickness of this particular ribbon, ≈45 nm. Finally, we also scanned the site by SEM immediately after scratching (Figure 3e) to capture loose items that would not have appeared in an AFM image; indeed, Figure 3e shows nanofibril ends pointing away from the surface. Thus, the AFM and SEM evidence presented in Figure 3 proves that the *Loxosceles* MA silk fibers entirely consist of nanofibrils. The cross-sectional dimensions of a nanofibril are ≈20 nm × 7 nm, which means that a typical ribbon (width 7 μm, thickness 50 nm) is made of ≈2500 nanofibrils. As a matter of fact, our work is the first demonstration that a silk fiber from any noncribellate spider species entirely consists of sub-100 nm diameter fibrils; cribellate spiders spin a quite different type of silk, a loose three-dimensional network of individual fibrils much thinner than 1 μm. As shown in the following, this has a profound impact on the understanding of the structure of silks and on the properties of silk nanofibrils, which have widely been postulated but never detected or characterized satisfyingly.

An important observation we made is that the ribbons exhibit a pronounced tendency to separate along the boundaries of nanofibrils (see white arrows in Figures 2a and 3e), suggesting that the bonding between nanofibrils is relatively weak. The fibrils' tendency to disjoin became even more evident when we used a focused ion beam (FIB) to cut a silk ribbon, as shown in the postcut in situ SEM image (Figure 4a, false-colored). Interestingly, the fracture area has an appearance akin to a ruptured piece of textile, with individual nanofibrils pointing in different directions away from the cutting site. Hence, our AFM and SEM evidence from ruptured, AFM-cut, and FIB-cut silk ribbons shows that the binding strength between the fibrils is small compared to the axial strength of the protein nanofibrils.

DOI: 10.1021/acsmacrolett.8b00678
ACS Macro Lett. 2018, 7, 1364−1370

Having established that the binding strength between the fibrils is weak, the length of the nanofibrils becomes critical for the fiber's mechanical performance. Short nanofibrils would likely cause premature failure, because they would slip before reaching their tensile strength, causing breakdown of the adhesive interface between nanofibrils. In this scenario, the fracture surfaces would show numerous pulled out nanofibrils, akin to what has been shown for the fracture surfaces of silk fibers of *Antheraea yamamai*.[28] However, none of our SEM or AFM data shows evidence for this type of failure. To the contrary, the AFM image of a ruptured ribbon featured in Figure 2a shows a fracture surface following an almost straight, ≈3 μm long line between points A and B, without any sign of pulled out nanofibrils. Thus, the nanofibrils are long enough that shear strength at the fibril−fibril interface was not the limiting factor, but rather the tensile strength of the nanofibrils themselves. In this scenario, the ribbon's mechanical performance is essentially the sum of the performance of the individual nanofibrils, and thus, the ribbon represents the mechanical properties of the average nanofibril.[24,25] A typical stress−strain curve of a *Loxosceles* ribbon is shown in Figure 4b featuring a strength of 0.90 GPa, an extensibility of 31% and a toughness >150 MJ/m^3, typical values for a good spider dragline silk.[2] The measured strength corresponds to a ribbon breaking force of 300 μN, meaning that each of the ≈2500 nanofibrils was loaded with ≈120 nN at break. Based on the same scaling, we normalized the stress−strain behavior to an individual nanofibril (second vertical axis on the right-hand side of Figure 4b).

For an experimental assessment of the nanofibril length we first used hexafluoroisopropanol (HFIP) to partially dissolve *Loxosceles* ribbons. Subsequently taken AFM images (Figure 4c,d) show how this procedure loosened the fibrillar arrangement. Most notably, these measurements revealed isolated nanofibrils from a native spider silk fiber for the first time, such as the nanofibril highlighted by white dashed lines in Figure 4d. This fibril was measured to be 1.38 μm long (see Figure S7 for another, 1.17 μm long fibril). Thus, we found the fibrils to be at least 10× longer than previously suggested.[29] Since HFIP may have contributed to breaking up and dissolving the fibrils, we expect them to be much longer in a native fiber. Indeed, our AFM images clearly resolve individual nanofibrils, and having reviewed dozens of high-resolution AFM images of *Loxosceles* ribbons we have not observed a single case of a fibril ending. This suggests the possibility that these nanofibrils extend through the entire ribbon. These observations are in line with our analysis of fracture surfaces, from which we concluded that the nanofibrils are long enough to prevent significant slippage.

Having isolated individual nanofibrils also allowed us to carry out an independent measurement of their cross-sectional dimensions. The average fibril width was 38.5 ± 6.2 nm (measured at the base of AFM cross sections); the average fibril height was 8.2 ± 2.4 nm (n = 7). These findings are in excellent agreement with our previous and more accurate dimensional analysis yielding 20 nm × 7 nm, once the broadening due to the size of the probe (r ≈ 8 nm) is taken into account. A sample cross-section is displayed as inset in Figure 4c; full experimental details are shown in the Supporting Information, section 2.6 and Figure S7.

Interestingly, the diameters of internal nanofibrils we observed matches the diameters of nanofibrils that had been observed on the fiber surface of several unrelated species.[15,16,18] And while the revealed surface nanofibrils only represent a negligible volume fraction of these fibers, it is quite possible that such nanofibrils play an important if not dominant role in the bulk of these fibers, too. Similarly, exfoliation of silkworm silk has recently revealed ≈20 nm diameter fibrils.[20] In a bottom-up approach, several works have demonstrated that nanofibrils can be self-assembled from reconstituted silk protein.[30−33] Our own work carried out with native silkworm protein has recently demonstrated that shear induces formation of 20 nm diameter fibrils from untreated, natural protein.[34,35] These nanofibrils we produced in vitro featured a general appearance very similar to all 20 nm diameter fibrils observed on the surfaces of natural silk fibers. Based on these observations we believe that there is an intrinsic self-assembly mechanism causing silk protein in general to form nanofibrils about 20 nm in diameter. We suspect that previous works reporting significantly thicker fibrils[9,10,19,36] were limited by imaging resolution or they had altered the fibrillar structure with preparation techniques too invasive for proteins. We further suggest that understanding the conditions of formation of these nanofibrils,[34,35] especially because we showed they are capable of achieving outstanding mechanical properties, may become important for the synthesis of artificial high-performance fibers inspired by silk.[37−39]

In summary, we have shown that *Loxosceles* MA silk fibers are entirely composed of ≈2500 close-packed, loosely bonded nanofibrils that are highly oriented, parallel to the fiber direction, with cross-sectional dimensions of 7 nm × 20 nm and lengths >1 μm. We detected isolated nanofibrils from a natural spider silk fiber for the first time, and determined their breaking strength to be ≈120 nN. Based on these observations on *Loxosceles* silk, we developed the most detailed structural model for any silk directly supported by experimental evidence, as shown in Figure 4e: (1) nanofibrils are the sole structural component, giving the silk fiber its strength; (2) the nanofibrils are loosely bound and aligned parallel to the fiber direction; (3) these nanofibrils are arranged in a "pseudo-layered" structure. Since the ribbons exhibit the outstanding mechanical properties typical of a good spider silk, we can draw several additional important conclusions from our model: the outstanding mechanical properties of *Loxosceles* ribbons are already implemented at the level of an individual nanofibril, challenging models employed for other spider silks. Some had suggested that the skin−core organization of silk fibers was needed to attain the mechanical properties typical of spider silk.[13,32] Others had considered silk fibers as semicrystalline polymer bodies with a three-dimensional distribution of crystalline regions in an amorphous matrix.[12,40,41] The *Loxosceles* ribbons exhibit outstanding properties based on a much simpler structural organization, entirely based on nanofibrils. The only remaining task toward a complete understanding of the hierarchical organization of this material virtually across all length scales will be to determine the organization of the silk protein within a nanofibril, identifying crystalline and amorphous regions, and so on. This will potentially have wide-ranging implications on the understanding of the structure−property relations of spider silk and on the engineering of silk-inspired high-performance fibers.

■ ASSOCIATED CONTENT

Supporting Information

The Supporting Information is available free of charge on the ACS Publications website at DOI: 10.1021/acsmacrolett.8b00678.

Detailed experimental methods (PDF).

DOI: 10.1021/acsmacrolett.8b00678
ACS Macro Lett. 2018, 7, 1364−1370

AUTHOR INFORMATION

Corresponding Author

*E-mail: schniepp@wm.edu.

ORCID

Hannes C. Schniepp: 0000-0003-4645-9469

Notes

The authors declare no competing financial interest.

ACKNOWLEDGMENTS

This material is based upon work supported by the National Science Foundation under Grant No. DMR-1352542. The authors thank Dr. Stephan Gerstl (ScopeM, ETH Zürich) for the focused ion beam work and Dr. Sean Koebley for tensile testing. We acknowledge Dr. Abigail Reft and Olga Trofimova for help with SEM imaging, and Rick Vetter for providing *Loxosceles* specimens. H.C.S. is deeply grateful to Fritz Vollrath for the introduction to silk and to the *Loxosceles* species.

REFERENCES

(1) Gosline, J.; Guerette, P.; Ortlepp, C.; Savage, K. The Mechanical Design of Spider Silks: From Fibroin Sequence to Mechanical Function. *J. Exp. Biol.* **1999**, *202* (23), 3295−3303.

(2) Agnarsson, I.; Kuntner, M.; Blackledge, T. A. Bioprospecting Finds the Toughest Biological Material: Extraordinary Silk from a Giant Riverine Orb Spider. *PLoS One* **2010**, *5* (9), e11234.

(3) Mittal, N.; Ansari, F.; Gowda, V. K.; Brouzet, C.; Chen, P.; Larsson, P. T.; Roth, S. V.; Lundell, F.; Wagberg, L. W.; Kotov, N. A.; Soderberg, L. D. Multiscale Control of Nanocellulose Assembly: Transferring Remarkable Nanoscale Fibril Mechanics to Macroscale Fibers. *ACS Nano* **2018**, *12* (7), 6378−6388.

(4) Matthews, J. A.; Wnek, G. E.; Simpson, D. G.; Bowlin, G. L. Electrospinning of Collagen Nanofibers. *Biomacromolecules* **2002**, *3* (2), 232−238.

(5) Naleway, S. E.; Porter, M. M.; McKittrick, J.; Meyers, M. A. Structural Design Elements in Biological Materials: Application to Bioinspiration. *Adv. Mater.* **2015**, *27* (37), 5455−5476.

(6) Ling, S.; Kaplan, D. L.; Buehler, M. J. Nanofibrils in Nature and Materials Engineering. *Nat. Rev. Mater.* **2018**, *3* (4), 18016.

(7) Ling, S.; Chen, W.; Fan, Y.; Zheng, K.; Jin, K.; Yu, H.; Buehler, M. J.; Kaplan, D. L. Biopolymer Nanofibrils: Structure, Modeling, Preparation, and Applications. *Prog. Polym. Sci.* **2018**, *85*, 1−56.

(8) Du, N.; Liu, X. Y.; Narayanan, J.; Li, L.; Lim, M. L. M.; Li, D. Design of Superior Spider Silk: From Nanostructure to Mechanical Properties. *Biophys. J.* **2006**, *91* (12), 4528−4535.

(9) Augsten, K.; Mühlig, P.; Herrmann, C. Glycoproteins and Skin-Core Structure in Nephila Clavipes Spider Silk Observed by Light and Electron Microscopy. *Scanning* **2000**, *22* (1), 12−15.

(10) Brown, C. P.; Harnagea, C.; Gill, H. S.; Price, A. J.; Traversa, E.; Licoccia, S.; Rosei, F. Rough Fibrils Provide a Toughening Mechanism in Biological Fibers. *ACS Nano* **2012**, *6* (3), 1961−1969.

(11) Pérez-Rigueiro, J.; Elices, M.; Plaza, G. R.; Guinea, G. V. Similarities and Differences in the Supramolecular Organization of Silkworm and Spider Silk. *Macromolecules* **2007**, *40* (15), 5360−5365.

(12) Silva, L. P.; Rech, E. L. Unravelling the Biodiversity of Nanoscale Signatures of Spider Silk Fibres. *Nat. Commun.* **2013**, *4*, 3014.

(13) Sponner, A.; Vater, W.; Monajembashi, S.; Unger, E.; Grosse, F.; Weisshart, K. Composition and Hierarchical Organisation of a Spider Silk. *PLoS One* **2007**, *2* (10), e998.

(14) Vollrath, F.; Holtet, T.; Thogersen, H. C.; Frische, S. Structural Organization of Spider Silk. *Proc. R. Soc. London, Ser. B* **1996**, *263* (1367), 147−151.

(15) Gould, S. A. C.; Tran, K. T.; Spagna, J. C.; Moore, A. M. F.; Shulman, J. B. Short and Long Range Order of the Morphology of Silk from Latrodectus Hesperus (Black Widow) as Characterized by Atomic Force Microscopy. *Int. J. Biol. Macromol.* **1999**, *24* (2−3), 151−157.

(16) Xu, G.; Gong, L.; Yang, Z.; Liu, X. Y. What Makes Spider Silk Fibers so Strong? From Molecular-Crystallite Network to Hierarchical Network Structures. *Soft Matter* **2014**, *10* (13), 2116−2123.

(17) Shen, Y.; Johnson, M. A.; Martin, D. C. Microstructural Characterization of Bombyx Mori Silk Fibers. *Macromolecules* **1998**, *31* (25), 8857−8864.

(18) Du, N.; Yang, Z.; Liu, X. Y.; Li, Y.; Xu, H. Y. Structural Origin of the Strain-Hardening of Spider Silk. *Adv. Funct. Mater.* **2011**, *21* (4), 772−778.

(19) Kitagawa, M.; Kitayama, T. Mechanical Properties of Dragline and Capture Thread for the Spider Nephila Clavata. *J. Mater. Sci.* **1997**, *32* (8), 2005−2012.

(20) Ling, S.; Li, C.; Jin, K.; Kaplan, D. L.; Buehler, M. J. Liquid Exfoliated Natural Silk Nanofibrils: Applications in Optical and Electrical Devices. *Adv. Mater.* **2016**, *28* (35), 7783−7790.

(21) Poza, P.; Pérez-Rigueiro, J.; Elices, M.; LLorca, J. Fractographic Analysis of Silkworm and Spider Silk. *Eng. Fract. Mech.* **2002**, *69*, 1035−1048.

(22) Jin, H.-J.; Kaplan, D. L. Mechanism of Silk Processing in Insects and Spiders. *Nature* **2003**, *424* (6952), 1057−1061.

(23) Lin, T.-Y.; Masunaga, H.; Sato, R.; Malay, A. D.; Toyooka, K.; Hikima, T.; Numata, K. Liquid Crystalline Granules Align in a Hierarchical Structure to Produce Spider Dragline Microfibrils. *Biomacromolecules* **2017**, *18*, 1350.

(24) Schniepp, H. C.; Koebley, S. R.; Vollrath, F. Brown Recluse Spider's Nanometer Scale Ribbons of Stiff Extensible Silk. *Adv. Mater.* **2013**, *25* (48), 7028−7032.

(25) Koebley, S. R.; Vollrath, F.; Schniepp, H. C. Toughness-Enhancing Metastructure in the Recluse Spider's Looped Ribbon Silk. *Mater. Horiz.* **2017**, *4*, 377−382.

(26) Knight, D. P.; Vollrath, F. Spinning an Elastic Ribbon of Spider Silk. *Philos. Trans. R. Soc., B* **2002**, *357* (1418), 219−227.

(27) Luria, J.; Kutes, Y.; Moore, A.; Zhang, L.; Stach, E. A.; Huey, B. D. Charge Transport in CdTe Solar Cells Revealed by Conductive Tomographic Atomic Force Microscopy. *Nat. Energy* **2016**, *1* (11), 16150.

(28) Zhang, W.; Ye, C.; Zheng, K.; Zhong, J.; Tang, Y.; Fan, Y.; Buehler, M. J.; Ling, S.; Kaplan, D. L. Tensan Silk-Inspired Hierarchical Fibers for Smart Textile Applications. *ACS Nano* **2018**, *12* (7), 6968−6977.

(29) Riekel, C.; Burghammer, M.; Dane, T. G.; Ferrero, C.; Rosenthal, M. Nanoscale Structural Features in Major Ampullate Spider Silk. *Biomacromolecules* **2017**, *18* (1), 231−241.

(30) Gong, Z.; Huang, L.; Yang, Y.; Chen, X.; Shao, Z. Two Distinct β-Sheet Fibrils from Silk Protein. *Chem. Commun.* **2009**, No. 48, 7506.

(31) Ling, S.; Li, C.; Adamcik, J.; Shao, Z.; Chen, X.; Mezzenga, R. Modulating Materials by Orthogonally Oriented β-Strands: Composites of Amyloid and Silk Fibroin Fibrils. *Adv. Mater.* **2014**, *26* (26), 4569−4574.

(32) Chen, Z.; Zhang, H.; Lin, Z.; Lin, Y.; van Esch, J. H.; Liu, X. Y. Programing Performance of Silk Fibroin Materials by Controlled Nucleation. *Adv. Funct. Mater.* **2016**, *26* (48), 8978−8990.

(33) Grant, A. M.; Kim, H. S.; Dupnock, T. L.; Hu, K.; Yingling, Y. G.; Tsukruk, V. V. Silk Fibroin-Substrate Interactions at Heterogeneous Nanocomposite Interfaces. *Adv. Funct. Mater.* **2016**, *26* (35), 6380−6392.

(34) Greving, I.; Cai, M.; Vollrath, F.; Schniepp, H. C. Shear-Induced Self-Assembly of Native Silk Proteins into Fibrils Studied by Atomic Force Microscopy. *Biomacromolecules* **2012**, *13* (3), 676−682.

(35) Koebley, S. R.; Thorpe, D.; Pang, P.; Chrisochoides, P.; Greving, I.; Vollrath, F.; Schniepp, H. C. Silk Reconstitution Disrupts Fibroin Self-Assembly. *Biomacromolecules* **2015**, *16* (9), 2796−2804.

(36) Putthanarat, S.; Stribeck, N.; Fossey, S. A.; Eby, R. K.; Adams, W. W. Investigation of the Nanofibrils of Silk Fibers. *Polymer* **2000**, *41* (21), 7735−7747.

(37) Xia, X.-X.; Qian, Z.-G.; Ki, C. S.; Park, Y. H.; Kaplan, D. L.; Lee, S. Y. Native-Sized Recombinant Spider Silk Protein Produced in Metabolically Engineered Escherichia Coli Results in a Strong Fiber. *Proc. Natl. Acad. Sci. U. S. A.* **2010**, *107* (32), 14059−14063.

DOI: 10.1021/acsmacrolett.8b00678
ACS Macro Lett. 2018, 7, 1364−1370

(38) Heidebrecht, A.; Eisoldt, L.; Diehl, J.; Schmidt, A.; Geffers, M.; Lang, G.; Scheibel, T. Biomimetic Fibers Made of Recombinant Spidroins with the Same Toughness as Natural Spider Silk. *Adv. Mater.* **2015**, *27* (13), 2189−2194.
(39) Andersson, M.; Jia, Q.; Abella, A.; Lee, X.-Y.; Landreh, M.; Purhonen, P.; Hebert, H.; Tenje, M.; Robinson, C. V.; Meng, Q.; Plaza, G. R.; Johansson, J.; Rising, A. Biomimetic Spinning of Artificial Spider Silk from a Chimeric Minispidroin. *Nat. Chem. Biol.* **2017**, *13*, 262−264.
(40) Simmons, A. H.; Michal, C. A.; Jelinski, L. W. Molecular Orientation and Two-Component Nature of the Crystalline Fraction of Spider Dragline Silk. *Science* **1996**, *271* (5245), 84−87.
(41) Sapede, D.; Seydel, T.; Forsyth, V. T.; Koza, M. M.; Schweins, R.; Vollrath, F.; Riekel, C. Nanofibrillar Structure and Molecular Mobility in Spider Dragline Silk. *Macromolecules* **2005**, *38* (20), 8447−8453.

DOI: 10.1021/acsmacrolett.8b00678
ACS Macro Lett. 2018, 7, 1364−1370